Absence of retbindin blocks glycolytic flux, disrupts metabolic homeostasis, and leads to photoreceptor degeneration

Tirthankar Sinha[a], Jianhai Du[b,c], Mustafa S. Makia[a], James B. Hurley[d], Muna I. Naash[a,1], and Muayyad R. Al-Ubaidi[a,1]

[a]Department of Biomedical Engineering, University of Houston, Houston, TX 77204; [b]Department of Ophthalmology, West Virginia University, Morgantown, WV 26506; [c]Department of Biochemistry, West Virginia University, Morgantown, WV 26506; and [d]Department of Biochemistry, University of Washington, Seattle, WA 98195

Edited by Claudio Punzo, University of Massachusetts Medical School, Worcester, MA, and accepted by Editorial Board Member Jeremy Nathans December 22, 2020 (received for review September 9, 2020)

We previously reported a model of progressive retinal degeneration resulting from the knockout of the retina-specific riboflavin binding protein, retbindin (*Rtbdn*$^{-/-}$). We also demonstrated a reduction in neural retinal flavins as a result of the elimination of RTBDN. Given the role of flavins in metabolism, herein we investigated the underlying mechanism of this retinal degeneration by performing metabolomic analyses on predegeneration at postnatal day (P) 45 and at the onset of functional degeneration in the P120 retinas. Metabolomics of hydrophilic metabolites revealed that individual glycolytic products accumulated in the P45 *Rtbdn*$^{-/-}$ neural retinas along with the elevation of pentose phosphate pathway, while TCA cycle intermediates remained unchanged. This was confirmed by using ^{13}C-labeled flux measurements and immunoblotting, revealing that the key regulatory step of phosphoenolpyruvate to pyruvate was inhibited via down-regulation of the tetrameric pyruvate kinase M2 (PKM2). Separate metabolite assessments revealed that almost all intermediates of acylcarnitine fatty acid oxidation, ceramides, sphingomyelins, and multiple toxic metabolites were significantly elevated in the predegeneration *Rtbdn*$^{-/-}$ neural retina. Our data show that lack of RTBDN, and hence reduction in flavins, forced the neural retina into repurposing glucose for free-radical mitigation over ATP production. However, such sustained metabolic reprogramming resulted in an eventual metabolic collapse leading to neurodegeneration.

retbindin | retinal degeneration | metabolism | flavins | metabolomics

Retbindin (RTBDN), with homology to chicken riboflavin binding protein, is exclusively expressed in the mammalian neural retina (NR) as a peripheral membrane protein (1). It specifically localizes at the interface of the NR and retinal pigment epithelium (RPE), where essential metabolites and nutrients are exchanged between the two layers (1). We have recently shown that the absence of RTBDN results in a progressive and a dose-dependent rod-and-cone functional decline starting as early as postnatal day (P) 120 (2). This functional decline was progressive and associated with reduced number of both rod (~37%) and cone (~45%) photoreceptors and minor structural abnormalities in the outer segments at P240 (2). Moreover, significant reduction in the levels of the two riboflavin-derived metabolic cofactors, flavin adenine dinucleotide (FAD) and flavin mononucleotide (FMN), was reported (2, 3).

The NR has one of the highest energy requirements in the body, and this is maintained via a unique metabolic symbiosis between the NR and the RPE (4–6). The initial glucose flux from the choroidal blood supply moves quickly through the RPE and into the NR to feed the highly glycolytic photoreceptors, which comprise about 60% of the total number of cells in NR (4, 7). In return, the NR provides the RPE with the lipid-rich outer segments and the glycolytic end product, lactate, a principal source of fuel for the RPE (8, 9). As expected, any factor that disrupts NR metabolism will in turn affect this symbiosis.

Given the widespread role of FAD and FMN in metabolism, in this study we set out to determine how elimination of RTBDN and the reduced flavin levels lead to retinal degeneration. We performed a comparative analysis of retinal metabolism between the retbindin knockout (*Rtbdn*$^{-/-}$) and age-matched wild-type (*WT*) animals before the onset (P45) and after the onset (P120) of functional decline.

Results

RTBDN Is Essential to Maintain Energy Homeostasis and Redox Potential of Both NR and RPE. We chose to perform our analyses on *Rtbdn*$^{-/-}$ and *WT* animals at P45, before the onset of functional decline, and right after the onset of functional decline at P120 (*SI Appendix*, Fig. S1). No significant histological and functional differences were detected between *Rtbdn*$^{-/-}$ and *WT* at P45 (*SI Appendix*, Fig. S1 *A–C*). Quantitative analyses of the rod-and-cone functional comparisons at P120 from both genotypes were previously reported (2), and their waveforms are shown in *SI Appendix*, Fig. S1*A*. Histological assessment of P120 retinas of the *Rtbdn*$^{-/-}$ (*SI Appendix*, Fig. S1 *B* and *C*) showed no

Significance

The retina has one of the highest energy requirements, and it harbors the highest flavins' content, essential factors for energy metabolism. It is unclear how the retina manages to preserve the high level of flavins, a topic for investigation. We recently reported a retinal riboflavin-binding protein, called retbindin. Here we report that absence of retbindin results in a significant reduction in retinal flavins, causing toxic metabolite buildup and triggering the retina to lend support to the impaired free-radical scavenging system by repurposing glucose. These have a domino effect, leading to reduced ATP synthesis and metabolic breakdown and results in retinal degeneration. This research emphasizes the role of metabolic changes as a primary cause behind retinal degeneration.

Author contributions: T.S., M.I.N., and M.R.A.-U. designed research; T.S. performed research; J.D., M.S.M., and J.B.H. contributed new reagents/analytic tools; T.S., M.I.N., and M.R.A.-U. analyzed data; and T.S., M.I.N., and M.R.A.-U. wrote the paper.

The authors declare no competing interest.

This article is a PNAS Direct Submission. C.P. is a guest editor invited by the Editorial Board.

[1]To whom correspondence may be addressed. Email: mnaash@central.uh.edu or malubaid@central.uh.edu.

This article contains supporting information online at https://www.pnas.org/lookup/suppl/doi:10.1073/pnas.2018956118/-/DCSupplemental.

Published February 1, 2021.

significant reduction in the number of photoreceptor nuclei in the outer nuclear layer. However, this reduction becomes prominent and statistically significant at P240 *Rtbdn*$^{-/-}$ (2).

We first evaluated levels of FAD and FMN in neural retina (NR) versus RPE–Choroid (RPE-Ch) of *Rtbdn*$^{-/-}$ and *WT* at P45 and compared to their levels at P120. Interestingly, retinal levels of both FAD (~70% of *WT*) and FMN (~65% of *WT*) were significantly reduced in P45 NR (Fig. 1 *A* and *B* and *SI Appendix*, Fig. S2), much earlier than the onset of functional decline seen at P120 (2). As expected, the reduction in NR levels of flavins was further exacerbated at P120 (~48% and ~46% of *WT*, respectively) (Fig. 1 *A* and *B* and *SI Appendix*, Fig. S2). This may indicate that the reduced availability of flavins at P45 is triggering the functional decline by affecting NR's energy metabolism way before its onset.

We recently showed that flavin levels are higher in the RPE than the NR of *WT* mice (3). Due to RTBDN localization at the tips of outer segments, we find that the ablation of RTBDN led to reduced levels of both FAD and FMN in the P45 RPE-Ch (~72% and ~57% of *WT*, respectively), followed by further decline at P120 (~35% and ~48% of *WT*, respectively) (Fig. 1 *A* and *B* and *SI Appendix*, Fig. S2). It is interesting that the reduction of FMN at P45 in the RPE-Ch was far greater (>10%) than in the NR, but nevertheless, the content of flavins still remained much higher in the RPE-Ch as in *WT* (*SI Appendix*, Fig. S2).

One of the earliest indicators of a disrupted metabolism is the levels of essential markers of metabolic activities. FAD and FMN are known to be essential cofactors for multiple catabolic reactions, especially those involved in energy metabolism (10). Furthermore, the electron transport chain is also inhibited if flavin availability is reduced (11). We next measured the ratios of ATP/ADP (Fig. 1*C*) and ATP/AMP (Fig. 1*D*), which together reflect if there is a difference in energy supply and demand. Interestingly, we found that both ATP/ADP (~84% of *WT*) and ATP/AMP (~77% of *WT*) ratios slightly, but yet, statistically significantly, reduced in the *Rtbdn*$^{-/-}$ NR at P45 and then further declined (~56% and ~43% of *WT*, respectively) at P120 (Fig. 1 *C* and *D*). The change in these ratios, although statistically insignificant, for the P45 RPE-Ch mirrored that of the NR, whereby the ATP/ADP ratio was 88% of *WT* and the ATP/AMP ratio was 86% of *WT*. These reductions became more obvious and statistically significant at P120 for both ATP/ADP and ATP/AMP (~64% and ~51% of *WT,* respectively) (Fig. 1 *C* and *D*). We also measured markers of cellular redox potential, NAD^+/NADH and $NADP^+$/NADPH (Fig. 1 *E* and *F*). We found that NAD^+/NADH is unaffected at P45, but significantly reduced at P120 for both NR and RPE-Ch (~64% and ~67% of *WT,* respectively) (Fig. 1*E*), further indicating inefficient energy metabolism. Similarly, $NADP^+$/NADPH ratio was unaffected at P45, but surprisingly, it was statistically significantly higher at P120 for both NR and RPE-Ch (~117% and ~130% of *WT*, respectively) (Fig. 1*F*),

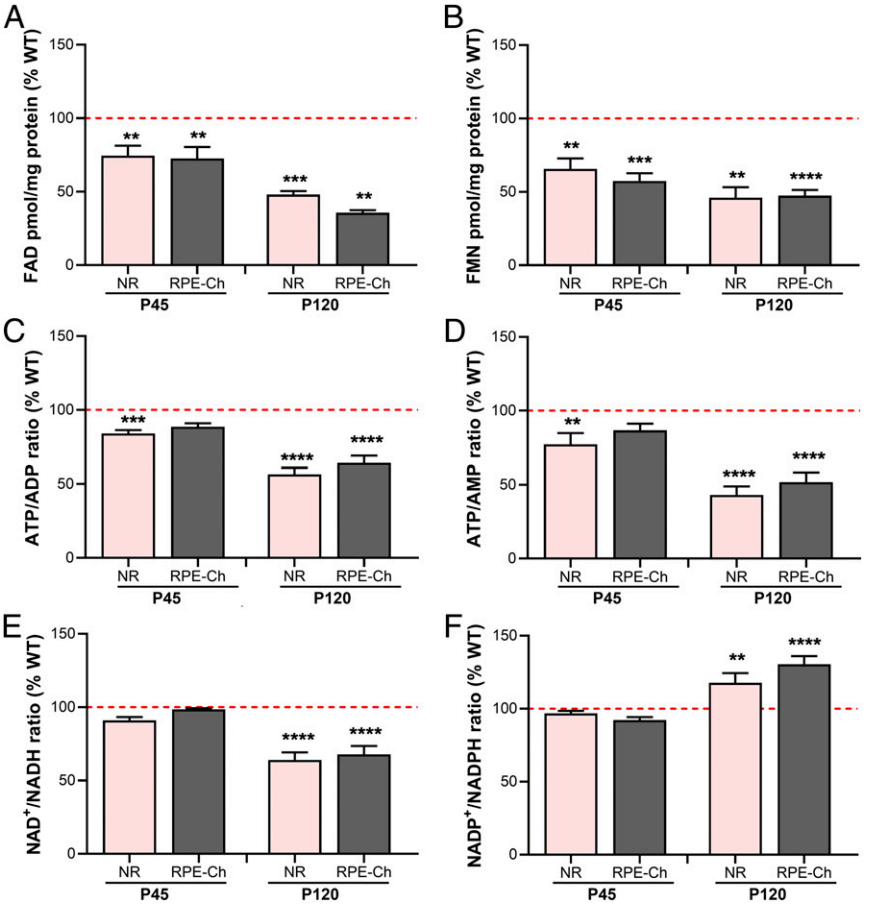

Fig. 1. RTBDN is critical for energy homeostasis and cellular redox potential of NR and RPE-Ch. Essential flavins like (*A*) FAD and (*B*) FMN and metabolite ratios of (*C*) ATP/ADP, (*D*) ATP/AMP, (*E*) NAD^+/NADH, and (*F*) $NADP^+$/NADPH, which are critical to evaluate the state of cellular homeostasis, were quantified in the neural retina NR and RPE-Ch of *Rtbdn*$^{-/-}$ and *WT* controls at P45 and P120. Values for *Rtbdn*$^{-/-}$ are presented as percent of age-matched *WT* (red dotted line is set at 100). Statistical comparisons were made between the *WT* and *Rtbdn*$^{-/-}$ for the individual metabolite of each tissue and at the respective ages. Tissues were collected as indicated in the *Materials and Methods* section, with $n = 10$ for *A* and *B* and $n = 6$ for *C*–*F*. Student's *t* test was used to determine significance, with $^{**}P < 0.01$, $^{***}P < 0.001$, and $^{****}P < 0.0001$. (NR, neural retina; RPE-Ch, RPE–Choroid).

reflecting a compromised cellular detoxification system. These results indicate that, unlike NR, none of the other cellular markers of metabolic homeostasis were significantly altered in the RPE-Ch at P45. Interestingly though, the changes in the RPE were almost equivalent to the changes in the NR at P120 (Fig. 1 *C–F*). Since the changes in NR begin earlier, this indicates that the initial dysregulation in NR metabolism is likely, leading to the heightened dysregulation in both NR and RPE at later ages.

Elimination of RTBDN Profoundly Impairs NR Glycolysis Followed by TCA Cycle, but Affects RPE to a Lesser Extent. Given the high-energy demands of the NR, it is not surprising that it harbors one of the highest flavin levels in the body along with the RPE (3). Nevertheless, how this is achieved has been a mystery until recently (1, 2), especially since any free riboflavin is rapidly cleared. It has been proposed that tissues, which maintain a barrier with the blood, often express unique riboflavin binding (or carrier) proteins to have a nascent pool of bound riboflavin available for metabolic turnover (12, 13). RTBDN presents itself as an excellent candidate for this in the retina. Therefore, we hypothesized that the reduction in flavin levels in absence of RTBDN could be enough to create a gap between the demand and supply ratio of flavins for the NR-RPE metabolic requirement.

To test this hypothesis, we took an untargeted global metabolomics approach and first quantified the steady state levels of metabolites in the RPE-Ch and the NR of *Rtbdn*$^{-/-}$ and *WT* mice at P45 and at P120. This should precisely identify the affected pathways by the elimination of RTBDN and those that are effected by the degeneration. One such pathway is glucose metabolism. In the P45 *Rtbdn*$^{-/-}$ NR, glucose, glucose–6-phosphate (G-6-P), and fructose–1,6-bisphosphate (F-1,6-BP) were significantly reduced to almost 50% of *WT* levels (Fig. 2 *A–C* and *I* and

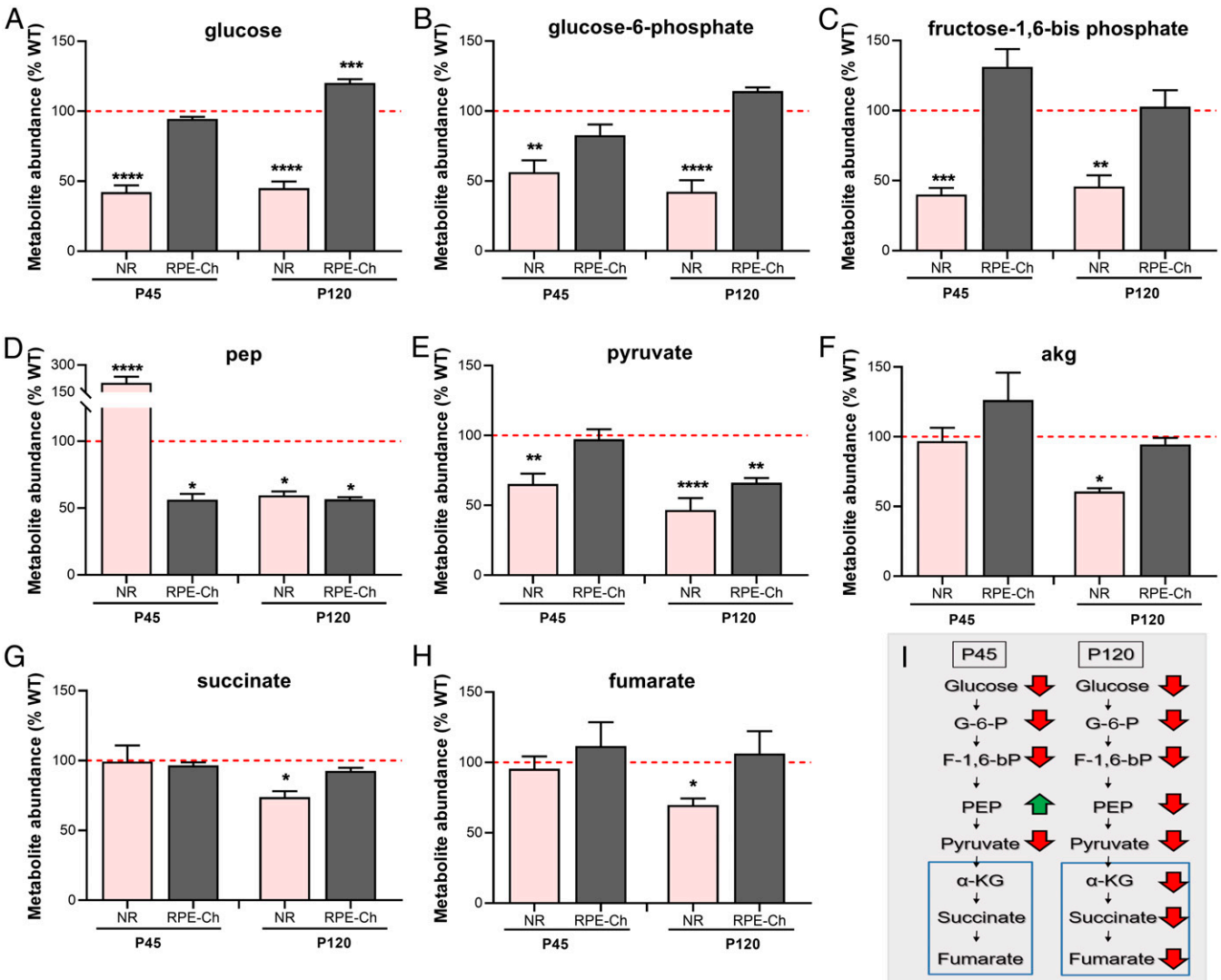

Fig. 2. Absence of RTBDN leads to reduced glycolysis at P45 followed by reduced TCA cycle at P120. Steady state levels of key glycolytic (*A–E*) and TCA cycle (*F–H*) metabolites were quantified in NR and RPE-Ch *Rtbdn*$^{-/-}$ and *WT* controls at P45 and P120. Tissues were collected as indicated in the *Materials and Methods* section, with $n = 10$ for *A–H*. The unit of *y* axis as metabolite abundance reflects the normalized metabolite concentration for the individual metabolite. Values are presented for *Rtbdn*$^{-/-}$ as percent of age-matched *WT* (red dotted line is set at 100). Statistical comparisons shown were made between the *WT* and *Rtbdn*$^{-/-}$ for the individual metabolite of each tissue at the respective ages. (*I*) A flowchart summarizing the changes in the NR, with the TCA cycle metabolites being marked with a blue box. Metabolites elevated in *Rtbdn*$^{-/-}$ are shown next to green arrows and those reduced are next to red arrows, while the ones lacking significant difference are unmarked. Student's *t* test was used to test significance, with $*P < 0.05$, $**P < 0.01$, $***P < 0.001$, and $****P < 0.0001$. (NR, neural retina; RPE-Ch, RPE–Choroid).

SI Appendix, Fig. S3 *A–C*). The generation of phosphoenolpyruvate (PEP) is a key step in glycolysis since it is followed by the transfer of phosphate from PEP to generate the second ATP and pyruvate. The levels of PEP were significantly elevated to >200% of the *WT* (Fig. 2 *D* and *I* and *SI Appendix*, Fig. S3*D*), while the pyruvate level is significantly reduced (~65% of *WT*) (Fig. 2 *E* and *I* and *SI Appendix*, Fig. S3*E*). The accumulation of PEP is likely a consequence of its slower conversion to pyruvate in the reaction catalyzed by pyruvate kinase. At P120, all steps leading to the formation of PEP in NR mimic the pattern observed at P45 (Fig. 2 *A–C* and *I* and *SI Appendix*, Fig. S3 *A–C*). However, there is much less PEP at P120 (<70% of *WT*) (Fig. 2 *D* and *I* and *SI Appendix*, Fig. S3*D*) than at P45. However, the steady state levels of the TCA cycle metabolites, α-ketoglutarate, succinate, and fumarate, were equivalent at P45 in *WT* and *Rtbdn*$^{-/-}$ NRs (Fig. 2 *F–H* and *I* and *SI Appendix*, Fig. S3 *F–H*), but they were significantly diminished at P120 *Rtbdn*$^{-/-}$ NRs (Fig. 2 *F–H* and *I*).

In the RPE-Ch, glycolysis up to the production of PEP was mainly unaffected by RTBDN deficiency (Fig. 2 *A–E* and *SI Appendix*, Fig. S3 *A–E*) at P45. In contrast to the NR, PEP levels were significantly reduced (<56% of *WT*) (Fig. 2*D* and *SI Appendix*, Fig. S3*D*), and pyruvate levels were equivalent to *WT* (Fig. 2*E* and *SI Appendix*, Fig. S3*E*). This may be due to the ability of the RPE to generate pyruvate from sources other than PEP, like lactate and pentose phosphate pathway, as well as by reductive carboxylation from the TCA cycle (4, 6, 14, 15). Surprisingly, the P120 *Rtbdn*$^{-/-}$ RPE-Ch seemed to be pushed into a high glucose state, with glucose levels being >120% of *WT* (Fig. 2*A* and *SI Appendix*, Fig. S3*A*). This could reflect a compensatory increase in glucose uptake in response to stress (16). However, as in the P120 *Rtbdn*$^{-/-}$ NR, the increase in RPE-Ch level of glucose likely is not sufficient to meet the cellular energy demand when PEP and pyruvate levels are significantly reduced to <60% of the *WT* (Fig. 2 *D* and *E* and *SI Appendix*, Fig. S3 *D* and *E*). TCA cycle metabolite levels in the RPE-Ch at both ages were unaffected (Fig. 2 *F–H* and *SI Appendix*, Fig. S3 *F–H*). This is in line with our (6) and others (8, 9) previous finding that compared to the NR, the RPE is more reliant on pathways other than glycolysis for energy production. Further, to understand if interim fuel repurposing can have a delayed detrimental effect on cellular metabolism, we asked whether this leads to amino acid catabolism in *Rtbdn*$^{-/-}$ NR and RPE-Ch at P120. As shown in *SI Appendix*, Fig. S4 *A* and *B*, the steady state levels of all essential amino acids were significantly reduced to <60% of *WT* values in both the *Rtbdn*$^{-/-}$ NR and RPE-Ch. Interestingly, many of these, like proline, arginine, and aspartic acid can serve as intermediate products of TCA cycle. Further, even intermediates of amino acid metabolism are significantly reduced (<75% of *WT*) in both tissues (*SI Appendix*, Fig. S4*B*), possibly indicating elevated catabolism.

RTBDN Absence Impedes Glycolytic Flux in the NR via Shift in PKM2 Oligomers. We next asked whether the reductions in the steady state levels of these metabolic intermediates in P45 *Rtbdn*$^{-/-}$ NR are caused by changes in the rate of their synthesis. Previous studies showed that RTBDN is exclusively expressed by the rods, while it is absent in the RPE (1). Thus, we hypothesized that the primary effect of RTBDN ablation would be on the NR. Unlike the NR, we did not observe any significant effect on glycolysis or TCA cycle of the RPE at P45, as demonstrated in Fig. 2. However, these changes become apparent on RPE glycolysis at P120. Since metabolic flux analysis and steady state levels may tell different story, and since the effect on RPE is secondary, we only focused on measuring the glucose flux in the NR at the pre-degeneration age. For this, we performed an ex vivo experiment by incubating NRs from P45 *Rtbdn*$^{-/-}$ and *WT* mice with ^{13}C-glucose as stated before (17) for 5 and 45 min and measured incorporation of ^{13}C in glycolytic and TCA cycle intermediates. Fig. 3*A* reflects a graphical representation depicting the flow of ^{13}C isotopologues (red circles) from [U-^{13}C] glucose through glycolysis and TCA cycle intermediates for a single span of the cycle (i.e., in 5 min). As shown in Fig. 3*B*, after 5 min, the level of the tracer in glyceraldehyde–3-phosphate (GAP) was >20 times higher in the *Rtbdn*$^{-/-}$ than the *WT*. Subsequently, the levels of the tracer in 3-phosphoglycerate and PEP were >3.5 times higher in *Rtbdn*$^{-/-}$ (Fig. 3*B*). In contrast, the tracer level in any of the following glycolytic or TCA cycle metabolites was less than half of the *WT* levels (Fig. 3*B*). The pattern observed with the 5-min incubation holds true for the 45-min incubation, with glucose flux being highly accumulated up to PEP formation and all the TCA cycle metabolites having significantly reduced incorporation of ^{13}C-glucose (Fig. 3*C*). These results clearly show that in the absence of RTBDN, glycolytic flux is inhibited, resulting in a significant reduction in the flow of glucose metabolic products into the TCA cycle.

In the NR, photoreceptors (both rods and cones) specifically express the most active key glycolysis regulator, pyruvate kinase M2 (PKM2) (18). Upon rod-specific deletion of PKM2, glycolytic flux in the NR is inhibited, and mice suffer from significant decline in rod function between P150 and P175 (19, 20). This is very similar to the *Rtbdn*$^{-/-}$ glycolytic flux measurements (Fig. 3) and can explain the steady state levels presented in Fig. 2. This also supports the hypothesis that the P45 *Rtbdn*$^{-/-}$ NR likely obtains TCA cycle intermediates from nonglycolytic sources in order to maintain *WT*-equivalent levels (Fig. 2 *F–H* and *SI Appendix*, Fig. S4 *A* and *B*). However, it is unclear why PEP accumulated early on (P45) in the absence of RTBDN. To investigate this, we measured the expression levels of the oligomers of PKM2 in the NR from P45 *Rtbdn*$^{-/-}$ animals. Although total PMK2 levels were the same in both *WT* and *Rtbdn*$^{-/-}$ retinas, the levels of the tetrameric complex of PKM2 were significantly reduced (<50% of *WT*) (Fig. 3 *D* and *E*). The tetrameric complex of PKM2 is the active form of the enzyme and is responsible for converting PEP to pyruvate. However, the dimeric form of PKM2 is required for two nonglycolytic functions: modulating cell death by translocating to the mitochondria and acting as a transcription factor by translocating to the nucleus (21, 22). We found both of the monomeric and dimeric forms of PKM2 slightly elevated in the *Rtbdn*$^{-/-}$ (Fig. 3 *D* and *E*). When we looked at the PKM2 oligomers at P120 (Fig. 3 *F* and *G*), we found the tetrameric PKM2 to be still reduced in *Rtbdn*$^{-/-}$ compared to the *WT*. Though interestingly, compared to the *WT* the dimer was also reduced in *Rtbdn*$^{-/-}$ now, possibly indicating transcriptional regulation as an effect of degeneration. However, the dimer:tetramer ratio still remained high in the *WT*, as in P45.

Reduction in Flavin Levels in *Rtdbn*$^{-/-}$ Compromises NR Free-Radical Scavenging and Triggers Glucose Repurposing to PPP. It has been previously shown that formation of the glycolytic PKM2 tetramer can be inhibited voluntarily by the cell under oxidative insult (21, 23–25). This helps the cell to prioritize free-radical scavenging and nucleotide biosynthesis over ATP production, by preventing glycolytic progression but boosting pentose phosphate pathway (PPP) (21, 23, 26, 27). In coherence with this, we found both the PPP end products (>125% of *WT*) and multiple intermediates of nucleotide biosynthesis were significantly elevated in the *Rtbdn*$^{-/-}$ NR at P45 (>125–200% of *WT*) (Fig. 4 *A* and *B* and *SI Appendix*, Fig. S4). In addition, several toxic intermediates of glutathione metabolism were also significantly elevated (>120–350% of *WT*), while the protective free-radical scavenger glutathione (GSH) was significantly reduced (<75% of *WT*) (Fig. 4*C*). This indicated that oxidative insult likely built up due to an imbalance in the free-radical scavenging system. Since one of the primary free-radical scavenging systems, the glutaredoxin system, is highly dependent on flavin availability and absence of RTBDN leads to

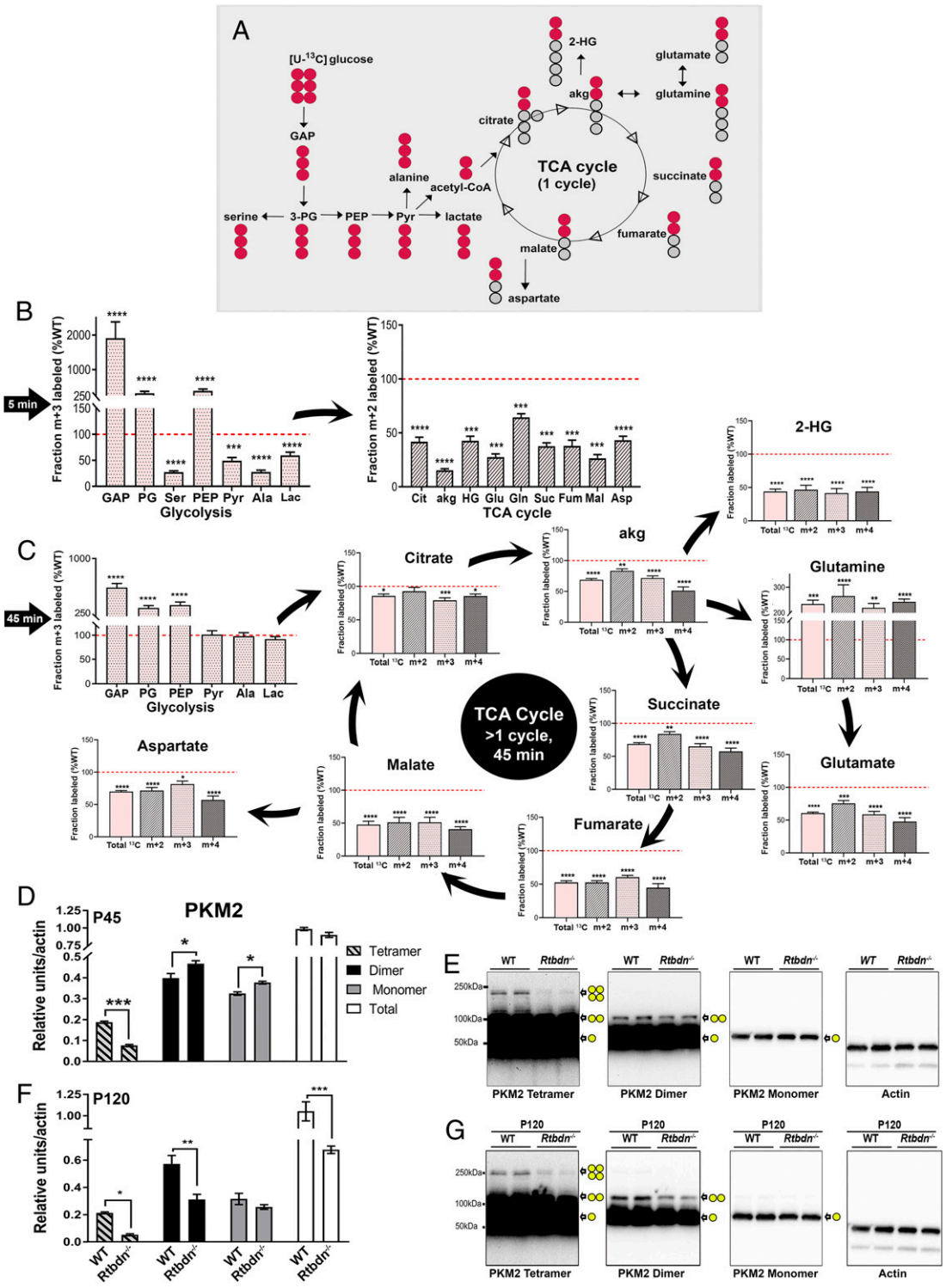

Fig. 3. RTBDN is required for sustaining glucose flux in the neural retina. (*A*) Flowchart depicting the flow of ^{13}C isotopologues (red circles) from [U-^{13}C] glucose through glycolysis and TCA cycle intermediates for a single span of the cycle. Circles represent the carbons in each intermediate. (*B*) Isotopologues were quantified for each glycolytic (m + 3) and TCA cycle (m + 2) metabolites after 5 min incubation with ^{13}C-glucose. (*C*) Isotopologues were quantified for each glycolytic (m + 3) and TCA cycle (m + 2, m + 3, m + 4, and total ^{13}C) metabolites after 45 min incubation with ^{13}C-glucose. Values are presented for *Rtbdn*$^{-/-}$ neural retina (P45) as percent of age-matched *WT* (red dotted line is set at 100). Statistical comparisons were made between the *WT* and *Rtbdn*$^{-/-}$ for the individual metabolite of each tissue at P45. Tissues were collected as indicated in the *Materials and Methods* section, with $n = 10$ for *B* and *C*. (*D*) Oligomers of PKM2 were quantified by densitometric analysis of various exposures of three independent immunoblots, each having two different samples from different mice at P45, for both *WT* and *Rtbdn*$^{-/-}$. (*E*) A representative immunoblot from P45 mice showing three different oligomers of PKM2 at increasing exposure times on the same immunoblot. (*F*) Densitometric analysis of PKM2 oligomers at P120 from different mice for both *WT* and *Rtbdn*$^{-/-}$ ($n = 6$) and (*G*) representative immunoblots showing three different oligomers of PKM2 from P120 mice. Subsequently, it was probed for actin, as shown. Yellow circles represent PKM2 forms of monomer, dimer, and tetramer at their individual localization on the immunoblot. All fold changes shown are significant (with $P < 0.0001$ using Student's *t* test) $*P < 0.05$, $**P < 0.01$, $***P < 0.001$, and $****P < 0.0001$.

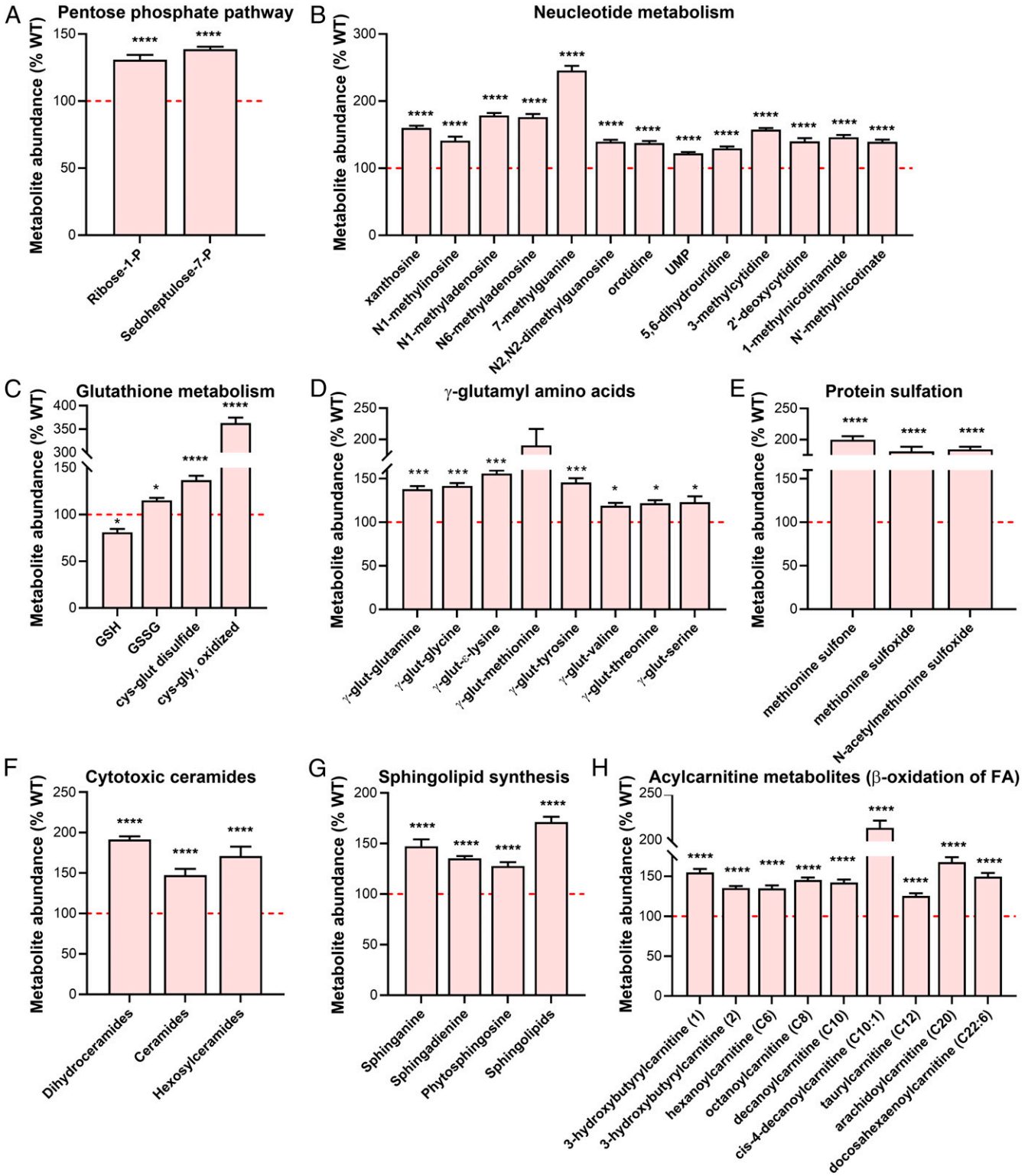

Fig. 4. RTBDN ablation up-regulates pentose phosphate pathway and nucleotide metabolism to meet the elevated need for free-radical scavenging, Percent changes in in the levels of pentose phosphate pathway, nucleotide metabolism, glutathione metabolism, free-radical markers, sphingolipid, and lipid metabolism intermediates in P45 *Rtbdn*$^{-/-}$ NR from *WT* control (marked by red dotted line at 100) are shown. (*A*) End products of pentose phosphate pathway. (*B*) Metabolic intermediates of nucleotide metabolism. (*C*) Reduced GSH and oxidized toxic intermediates of glutathione metabolism. (*D*) Amino acids modified by γ-glutamyl. (*E*) Sulfonated methionine residues. (*F*) Toxic ceramide metabolites. (*G*) Intermediates of sphingolipid biosynthesis. (*H*) Intermediates of β-oxidation of fatty acids marked by acylcarnitine. Each group has $n = 6$–9 independent preparations. Two-way ANOVA was used to determine significance, with $*P < 0.05$, $***P < 0.001$, and $****P < 0.0001$. (UMP, uridine monophosphate; GSH, reduced glutathione; GSSG, oxidized glutathione.)

50% reduction in flavin levels in the NR, we hypothesized that this results in gradual accumulation of reactive oxygen species, which eventually causes the oxidative insult endogenously. Reduced flavins are well documented to result in poor recycling of GSH, as glutathione reductase needs flavin as a cofactor (28). In further validation of this proposed endogenous accumulation of oxidative insult, we found multiple amino acids to have been γ-glutamyl–modified (Fig. 4*D*) and to have elevated levels of methionine sulfonation (Fig. 4*E*), both of which are robust markers of early stages of protein oxidation as a result of oxidative insult (29, 30).

When serine is adequately available, sphingosine is converted to the neuroprotective sphingosine–1-phosphate (S1P). However, during serine deficiency, alanine is incorporated into sphingolipids to generate toxic ceramides (31–33). Since we previously found serine biosynthesis also significantly reduced (~27% of *WT*) (Fig. 3*B*), we wondered if cytotoxic ceramides might be adding to this oxidative stress. All the di-hydroceramides and their cytotoxic end products, hexasylceramides, were significantly elevated (>150% of *WT*) (Fig. 4*F*). Similar to the known fact that reduced flavins can impede lipid metabolism, as multiple acyl-co-A dehydrogenases are flavin-dependent, we found sphingolipid synthesis and acyl carnitine intermediates were all significantly accumulated (>120–200% of *WT*) in the *Rtbdn*$^{-/-}$ NR, leading to inefficient lipid processing (Fig. 4 *G* and *H*). It is important to note that our interpretation of elevated sphingolipids and ceramides as toxic accumulation in the NR at P45 is different from our interpretation of elevated glucose levels in the RPE at P120, as reported in Fig. 2*A*. We show in Fig. 2 that only glucose was elevated in the RPE, while G-6-P and F-1,6-BP both were unchanged. This indicated that elevation in glucose levels was not a result of reduction in conversion to G-6-P but potentially an effect of increased glucose uptake due to stress, as explained earlier. It has been previously shown that at the onset of degeneration, RPE up-regulates glucose uptake and provides lesser glucose to the NR (16). This is in sync with our interpretation of the rest of the steady state data for both NR and RPE as well. However, for the sphingolipids (Fig. 4*G*), not only the initial metabolite (sphinganine) but the intermediates (sphingadienine and phytosphingosine) as well as the end product (sphingolipids) of the synthesis pathway were elevated in the NR at P45. This indicated that unlike glucose, which can be taken up from exogenous sources, sphingolipids and ceramides, both of which need to be biosynthesized, are accumulating in the form of end products of the biosynthetic pathway (Fig. 4 *G* and *H*). Previous work by others has shown that such accumulation of sphingolipids and ceramides are toxic to the NR (32–35). These earlier metabolic alterations at P45 may be adding to the impaired free-radical scavenging in the absence of Rtbdn, eventually leading to the cumulative metabolic collapse we observed at P120 (Fig. 2).

Discussion

In our previous work, we demonstrated an age-dependent decline in flavins' levels concomitant with a reduction in retinal function and structure (3). This indicates that the energy-consuming functional response of the NR is also influenced by flavin homeostasis. Furthermore, flavin levels are significantly diminished in various models of rod-specific degeneration, and absence of RTBDN expedites the cone-rod dystrophy in an animal model (3, 36). These further confirm the importance of flavins' homeostasis for the health of the NR, primarily of the photoreceptors. In the current study, we identified the causes behind the degenerative phenotype associated with the ablation of RTBDN by demonstrating that reduction in flavins resulted in impaired glutathione recycling as well as toxic metabolite buildup and increased methionine sulfonation (Fig. 5). In addition, in the absence of glucose flux through serine biosynthesis, sphingolipid metabolism gets adversely affected, and toxic hexasylceramide accumulates. This triggers the NR to impede glycolytic progression via inhibition of tetrameric PKM2 formation and rather up-regulate PPP to mitigate this oxidative stress. In presence of reduced flavin cofactors, lipolysis cannot function efficiently also, leading to acylcarnitine buildup in the *Rtbdn*$^{-/-}$ NR (Fig. 5). Furthermore, as the metabolic load increases, the ATP demand

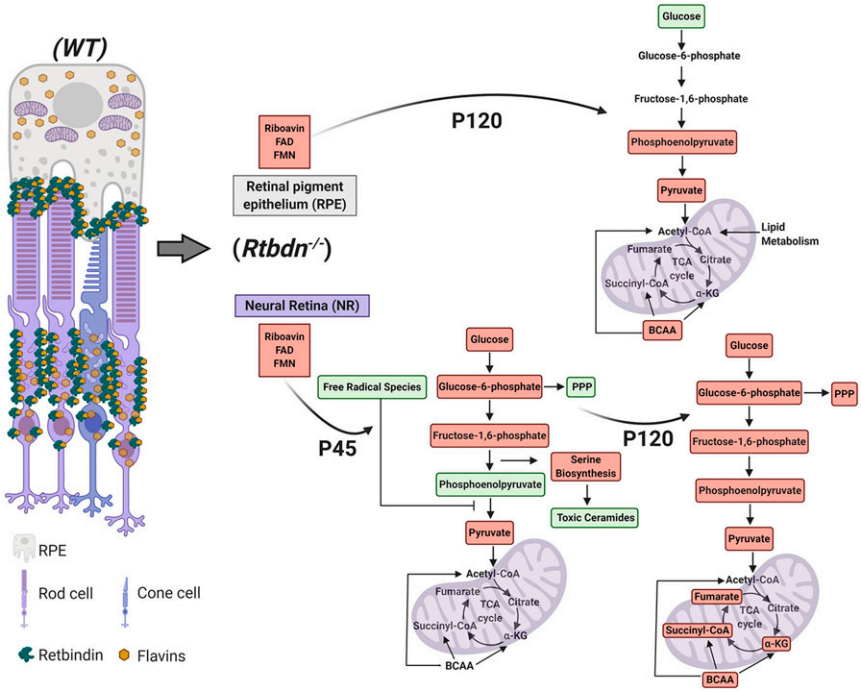

Fig. 5. Graphical representation of the effect of RTBDN ablation on NR-RPE metabolic homeostasis. Localization of RTBDN-bound flavin is shown in the *WT* neural retina–RPE junction and in the photoreceptor inner segment. In its absence, the resulting metabolic abnormalities in neural retina at P45 and P120 and in RPE at P120 are shown. Peach boxes represent significant reduction, while green boxes represent significant elevation.

and supply gap widens and disrupts metabolic homeostasis. This coincides with severe loss of amino acid metabolism in the *Rtbdn*$^{-/-}$ NR and RPE (Fig. 5).

Even though it has been shown that loss of PKM2 (*Pkm2*$^{-/-}$) can lead to retinal degeneration, the mechanism is yet unknown (37). It is assumed that since the photoreceptors are chiefly glycolytic in the absence of PKM2, their anabolism is compromised (37). Here we show that RTBDN ablation can affect the rate of glycolysis in a similar manner as *Pkm2*$^{-/-}$, but promoting PPP to meet the enhanced need of free-radical scavenging only serves as a short-term coping mechanism, and soon degeneration ensues. This strategy seems partially similar to therapeutic approaches suggested for acute stress conditions (20, 38). An important feature of our research is that it determined the factors that precede, and may lead to, functional decline and eventual degeneration, providing critical insights into the primary causes behind retinal degeneration. It is important to note though, that all our metabolomics analyses were performed at a specific time of the day, while a time course across different times of the day may yield even more insightful information, especially with reference to RPE health. Our future experiments will consider these types of studies. Nevertheless, the results presented here further emphasize that subtle changes in retinal metabolic homeostasis can skew the balance between physiology and pathology and eventually impact retinal function directly.

Materials and Methods

Additional information for each section is in *SI Appendix*.

Animals. *Rtbdn*$^{-/-}$ animals were generated as previously described (2). All animal experiments were approved by the University of Houston Institutional Animal Care and Use Committee and adhered to recommendations in the NIH *Guide for the Care and Use of Laboratory Animals* (39) and the Association for Research in Vision and Ophthalmology.

Tissue Collection. Mice were anesthetized by intramuscular injection of 85 mg/kg ketamine and 14 mg/kg xylazine. Using forceps and tweezers, the NR was extracted, and the rest of the eyecup was carefully removed. The RPE-Ch was carefully scraped out of the eyecup, quickly extracted, rinsed in phosphate-buffered saline (pH 7.4), and immediately frozen in liquid nitrogen. NR and RPE-Ch samples used for the steady state metabolomic analyses shown in Figs. 1 *C*–*E*, 2, and 4 and *SI Appendix*, Fig. S4 were pooled from six nonlittermates, normalized to their respective protein concentration, and considered as a single sample. Data presented are from six independent measurements for each (n = 6). Samples analyzed for *SI Appendix*, Fig. S3 were pooled from a single animal (two retinas and their corresponding RPE-Ch from one animal), normalized to their respective protein concentration and considered as a single sample, and data are presented from three independent measurements (n = 3). Metabolite flux measurements shown in Fig. 3 and results in Fig. 1 *A* and *B* and *SI Appendix*, Fig. S2 were from 10 independent measurements (n = 10) each of a single NR or RPE-Ch from individual animals.

Metabolomics Sample Preparation and Analysis. Samples were prepared and metabolomics analyses were done as described previously (6).

^{13}C Labeling and Measurements by GC-MS. Collected fresh neural retinas were immediately incubated in newly prepared Krebs–Ringer–Bicarbonate buffer as an ex vivo culture, along with U–^{13}C-glucose (5 mM) for 5 min and 45 min. Each reaction was stopped by transferring individual neural retina to cold 0.9% NaCl solution and was subsequently frozen. Each sample thereafter was processed and analyzed as described (4, 40).

High-Performance Liquid Chromatography and Quantification of Flavins. For flavin quantification, a previously described method was followed (3).

Immunoblot Analysis. Immunoblot analysis was performed on total retinal extracts under nonreducing SDS-PAGE conditions and probed with anti-PKM2 (CS04661) and anti-actin antibodies (21). Chemiluminescence imaging of the immunoblot was done at increasing exposure times (increment of 30 s) to identify the individual oligomers on the same immunoblot. Densitometric analysis was done of multiple exposures to quantify the presence of the respective bands. PKM2 monomer and dimer saturated in early and medium exposures, respectively, while tetramer took longer exposure to be saturated on the same immunoblot.

Statistical Analysis. ANOVA contrasts were used to identify significant ($P \leq 0.05$) differences between the experimental groups. An estimate of the false discovery rate (q-value) was also calculated to take into account the multiple comparisons that normally occur in metabolomic-based studies.

Data Availability. All study data are included in the article and/or supporting information.

ACKNOWLEDGMENTS. This study was supported by grants from the National Eye Institute (EY026499 and EY026030). Graphical representation images were created in Biorender.com.

1. R. A. Kelley, M. R. Al-Ubaidi, M. I. Naash, Retbindin is an extracellular riboflavin-binding protein found at the photoreceptor/retinal pigment epithelium interface. *J. Biol. Chem.* **290**, 5041–5052 (2015).
2. R. A. Kelley *et al.*, Ablation of the riboflavin-binding protein retbindin reduces flavin levels and leads to progressive and dose-dependent degeneration of rods and cones. *J. Biol. Chem.* **292**, 21023–21034 (2017).
3. T. Sinha, M. Makia, J. Du, M. I. Naash, M. R. Al-Ubaidi, Flavin homeostasis in the mouse retina during aging and degeneration. *J. Nutr. Biochem.* **62**, 123–133 (2018).
4. M. A. Kanow *et al.*, Biochemical adaptations of the retina and retinal pigment epithelium support a metabolic ecosystem in the vertebrate eye. *eLife* **6**, e28899 (2017).
5. B. S. Winkler, Glycolytic and oxidative metabolism in relation to retinal function. *J. Gen. Physiol.* **77**, 667–692 (1981).
6. T. Sinha, M. I. Naash, M. R. Al-Ubaidi, The symbiotic relationship between the neural retina and retinal pigment epithelium is supported by utilizing differential metabolic pathways. *iScience* **23**, 101004 (2020).
7. A. Swarup *et al.*, Modulating GLUT1 expression in retinal pigment epithelium decreases glucose levels in the retina: Impact on photoreceptors and Müller glial cells. *Am. J. Physiol. Cell Physiol.* **316**, C121–C133 (2019).
8. J. Adijanto *et al.*, The retinal pigment epithelium utilizes fatty acids for ketogenesis. *J. Biol. Chem.* **289**, 20570–20582 (2014).
9. J. Reyes-Reveles *et al.*, Phagocytosis-dependent ketogenesis in retinal pigment epithelium. *J. Biol. Chem.* **292**, 8038–8047 (2017).
10. H. J. Powers, Riboflavin (vitamin B-2) and health. *Am. J. Clin. Nutr.* **77**, 1352–1360 (2003).
11. N. Gregersen, W. Rhead, E. Christensen, Riboflavin responsive glutaric aciduria type II. *Prog. Clin. Biol. Res.* **321**, 477–494 (1990).
12. K. Muniyappa, P. R. Adiga, Occurrence and functional importance of a riboflavin-carrier protein in the pregnant rat. *FEBS Lett.* **110**, 209–212 (1980).
13. S. S. Visweswariah, P. R. Adiga, Purification of a circulatory riboflavin carrier protein from pregnant bonnet monkey (*M. radiata*): Comparison with chicken egg vitamin carrier. *Biochim. Biophys. Acta* **915**, 141–148 (1987).
14. J. Du *et al.*, Reductive carboxylation is a major metabolic pathway in the retinal pigment epithelium. *Proc. Natl. Acad. Sci. U.S.A.* **113**, 14710–14715 (2016).
15. J. B. Hurley, K. J. Lindsay, J. Du, Glucose, lactate, and shuttling of metabolites in vertebrate retinas. *J. Neurosci. Res.* **93**, 1079–1092 (2015).
16. W. Wang *et al.*, Metabolic deregulation of the blood-outer retinal barrier in retinitis pigmentosa. *Cell Rep.* **28**, 1323–1334.e4 (2019).
17. J. Du, J. D. Linton, J. B. Hurley, Probing metabolism in the intact retina using stable isotope tracers. *Methods Enzymol.* **561**, 149–170 (2015).
18. K. J. Lindsay *et al.*, Pyruvate kinase and aspartate-glutamate carrier distributions reveal key metabolic links between neurons and glia in retina. *Proc. Natl. Acad. Sci. U.S.A.* **111**, 15579–15584 (2014).
19. A. Rajala *et al.*, Pyruvate kinase M2 regulates photoreceptor structure, function, and viability. *Cell Death Dis.* **9**, 240 (2018).
20. T. J. Wubben *et al.*, Photoreceptor metabolic reprogramming provides survival advantage in acute stress while causing chronic degeneration. *Sci. Rep.* **7**, 17863 (2017).
21. Y. Wang *et al.*, *O*-GlcNAcylation destabilizes the active tetrameric PKM2 to promote the Warburg effect. *Proc. Natl. Acad. Sci. U.S.A.* **114**, 13732–13737 (2017).
22. T. Li *et al.*, PKM2 coordinates glycolysis with mitochondrial fusion and oxidative phosphorylation. *Protein Cell* **10**, 583–594 (2019).
23. D. Anastasiou *et al.*, Inhibition of pyruvate kinase M2 by reactive oxygen species contributes to cellular antioxidant responses. *Science* **334**, 1278–1283 (2011).
24. D. Anastasiou *et al.*, Pyruvate kinase M2 activators promote tetramer formation and suppress tumorigenesis. *Nat. Chem. Biol.* **8**, 839–847 (2012).
25. R. V. S. Rajala, Aerobic glycolysis in the retina: Functional roles of pyruvate kinase isoforms. *Front. Cell Dev. Biol.* **8**, 266 (2020).
26. N. M. Grüning *et al.*, Pyruvate kinase triggers a metabolic feedback loop that controls redox metabolism in respiring cells. *Cell Metab.* **14**, 415–427 (2011).

27. A. Stincone *et al*., The return of metabolism: Biochemistry and physiology of the pentose phosphate pathway. *Biol. Rev. Camb. Philos. Soc.* **90**, 927–963 (2015).
28. E. Beutler, Effect of flavin compounds on glutathione reductase activity: In vivo and in vitro studies. *J. Clin. Invest.* **48**, 1957–1966 (1969).
29. G. Kim, S. J. Weiss, R. L. Levine, Methionine oxidation and reduction in proteins. *Biochim. Biophys. Acta* **1840**, 901–905 (2014).
30. G. Koenig, S. Seneff, Gamma-glutamyltransferase: A predictive biomarker of cellular antioxidant inadequacy and disease risk. *Dis. Markers* **2015**, 818570 (2015).
31. M. V. Simón, F. H. Prado Spalm, M. S. Vera, N. P. Rotstein, Sphingolipids as emerging mediators in retina degeneration. *Front. Cell. Neurosci.* **13**, 246 (2019).
32. M. Stiles *et al*., Sphingolipid profile alters in retinal dystrophic P23H-1 rats and systemic FTY720 can delay retinal degeneration. *J. Lipid Res.* **57**, 818–831 (2016).
33. T. E. Fox *et al*., Diabetes alters sphingolipid metabolism in the retina: A potential mechanism of cell death in diabetic retinopathy. *Diabetes* **55**, 3573–3580 (2006).
34. R. S. Brush *et al*., Retinal sphingolipids and their very-long-chain fatty acid-containing species. *Invest. Ophthalmol. Vis. Sci.* **51**, 4422–4431 (2010).
35. N. P. Rotstein, G. E. Miranda, C. E. Abrahan, O. L. German, Regulating survival and development in the retina: Key roles for simple sphingolipids. *J. Lipid Res.* **51**, 1247–1262 (2010).
36. A. M. Genc *et al*., Elimination of a retinal riboflavin binding protein exacerbates degeneration in a model of cone-rod dystrophy. *Invest. Ophthalmol. Vis. Sci.* **61**, 17 (2020).
37. Y. Chinchore, T. Begaj, D. Wu, E. Drokhlyansky, C. L. Cepko, Glycolytic reliance promotes anabolism in photoreceptors. *eLife* **6**, e25946 (2017).
38. T. J. Wubben *et al*., Small molecule activation of metabolic enzyme pyruvate kinase muscle isozyme 2, PKM2, circumvents photoreceptor apoptosis. *Sci. Rep.* **10**, 2990 (2020).
39. National Research Council, *Guide for the Care and Use of Laboratory Animals* (National Academies Press, Washington, DC, 8th Ed., 2011).
40. M. Yam *et al*., Proline mediates metabolic communication between retinal pigment epithelial cells and the retina. *J. Biol. Chem.* **294**, 10278–10289 (2019).